PNNL-37213

Milestone Report

Integration of the fundamental knowledge on solvent-packing interactions into the multiscale framework for column scale design and optimization.

Work Performed Under
Activity Number 0004000.6.600.007.002 ARRA

Prepared by
Pacific Northwest National Laboratory
Richland, Washington 99352

Prepared for the
U.S. Department of Energy
National Energy Technology Laboratory

December 2024

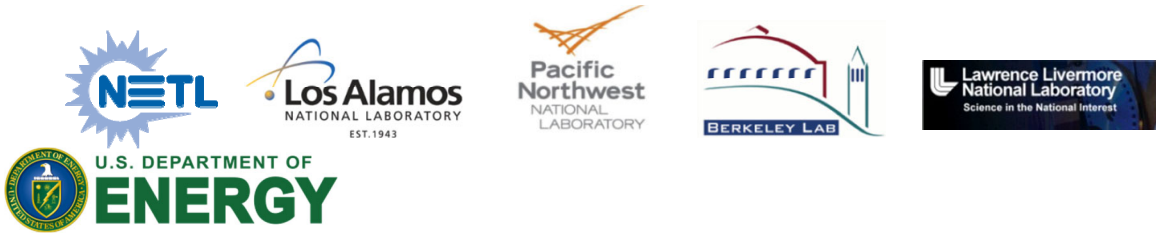

Revision Log

Revision	Date	Revised By:	Description
1.0	12/20/2023	Rajesh Singh	1st draft
2.0	12/31/2024	Yucheng Fu	2nd Draft
2.1	12/31/2024	Rajesh Singh	2nd Draft
2.3	12/31/2024	Zhijie Xu	Editing

Disclaimer

Acknowledgment of Funding

This project was funded under the Carbon Capture Simulation for Industry Impact ($CCSI^2$) under the following FWPs and contracts:

PNNL–68494

Contents

List of Figures

List of Tables

Integration of the fundamental knowledge on solvent-packing interactions into the multiscale framework for column scale design and optimization

Rajesh Kumar Singh, Yucheng Fu, Zirui Mao, Yuan Jiang, Jennifer Yao, Dushyant Barpaga, Jie Bao and Zhijie Xu

Pacific Northwest National Laboratory, Richland, WA 99352, USA

Executive Summary

The interfacial area, also known as the effective mass transfer area, is a key factor for determining the mass transfer for carbon dioxide (CO_2) capture via the chemical absorption process in a packed column, and thus the overall capture efficiency of the packed column. Most of the widely used empirical and semi-empirical models for interfacial area were derived indirectly through absorption mass transfer with simplifications based on fast chemical kinetics. This report presents the comprehensive unique multiscale approach to develop a surrogate model for effective mass transfer area in structured packed columns that accounts local hydrodynamics as well as variation in physical properties, and changes in packing surface characteristics. The effective contact angle on the packing surface, which describes the packing surface and solvent interaction, was measured using the modified Wilhelmy plate method accounting the physical properties of solvent, CO_2 loading, and temperature. Next, a comprehensive CFD simulation campaign based on the design of experiments (DOE) were performed to derive a surrogate model of the effective mass transfer area that takes into consideration the physical properties of solvent, contact angle, local hydrodynamics, etc. The developed surrogate model was integrated into the ASPEN PLUS process modelling via a compiled FORTRAN subroutine in form of .dll file. This surrogate integration with the into process modelling takes into account the effective mass transfer area in order to capture CO_2 absorption in each stage of the column. The present multiscale approach has advantage of two-way coupling i.e. interchanging information both direction: 1, ASPEN PLUS to surrogate model (temperature,

physical properties, CO_2 loading, etc., at each stage) and 2. Surrogate model computes the effective mass transfer area for determining CO_2 absorption. This unique and promising capability can aid process modeling to accelerating the carbon capture technology at column scale, particularly supporting large scale pilot experiments.

Graphical Summary

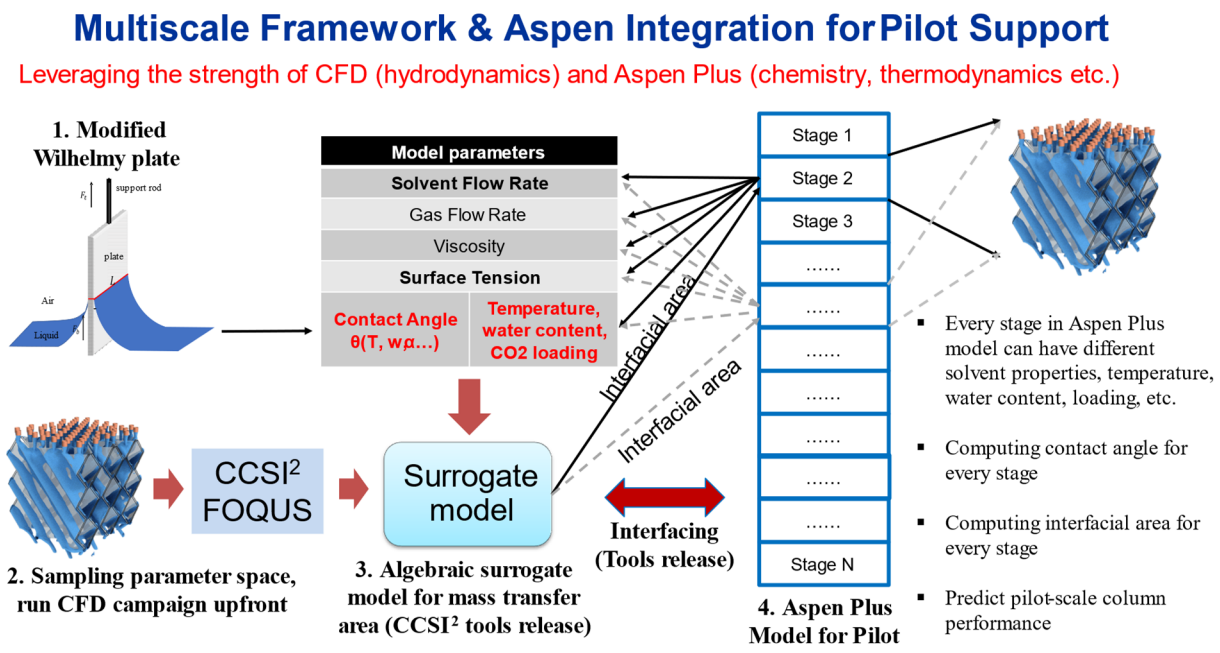

1. Introduction and Background

Carbon dioxide (CO_2) is the most important greenhouse gas (approximately 66% of the radiative forcing by the long-lived greenhouse gases) in the atmosphere that absorbs and radiates incoming solar radiation to earth surface, consequently heating the lower atmosphere [1]. Efforts for limiting anthropogenic warming to 1.5°C was crucial declaration of the Paris Agreement [2]. Fossil fuel CO_2 emissions have consistently increased during the last couple of decades, with coal-fired power plants as the primary source of CO_2 emissions [3, 4]. Therefore, reducing the emission is essential to mitigate the impacts of the global climate challenge. Solvent absorption based carbon capture system (CCS) can be a promising technology in power plants among the various available technologies [5]. The absorption is carried out using countercurrent gas–liquid flows in a packed column for enhancing effective mass transfer area. Structured packing provides a large surface area for mass transfer between the phases with minimum pressure drop across the column [5]. A structured packing is generally made of corrugated sheets arranged in a crisscross fashion that combine to form a single layer of the packing element. The column is filled with multiple layers of these packing units that are rotated with respect to one another. The hydrodynamic performance of a packed column is complex and is determined by various factors such as solvent properties, liquid and gas loads, packing surface features, column design, etc. Therefore, a better understanding of hydrodynamics particularly effective mass transfer area/ interfacial area would aid in packed column design and operation optimization. In this context, computational fluid dynamic (CFD) simulation can be leveraged during the design phase to achieve economic and efficient solutions. It is worth noting that CFD does not replace the experiments, but it can reduce the number of experiments required while also complementing the setup and analysis. CFD has been receiving recognition for investigating the hydrodynamic characteristics in structured packings over the last couple of decades [9-13]

Structure packed columns have length scales of several meters, diameter ranging from 5 to10 meters, and column heights of 20 to 30 meters [6, 7]. In comparison, the packing's characteristic dimensions are significantly smaller, with typical layer of corrugated structured packing measuring approximately 20 centimeters in length. Furthermore, thickness of liquid film thickness is measured in the order of tenth of millimeters. These underlying phenomenon in these length scales cannot be simultaneously resolved in a single computational model; that is, it is computationally infeasible to perform computational simulations while accounting for local gas-liquid interactions and packing geometry. As a result, a multi-scale strategy is necessary including micro, meso and macro scales [7]. This strategy can provide useful insights into the hydrodynamic behavior at different scales, with studies of interfacial area often being considered at the packing geometry level.

Interfacial area/effective mass transfer area is a critical factor for absorption efficiency, and maximum interfacial area in a packed column is desirable to improve column efficiency. Interfacial area generally reflects the solvent flow pattern within the commercial column. Consequently, several experimental and computational efforts have been reported. Using chemical absorption, Tsai et al [8-11] investigated the effect of viscosity on interfacial area as a function of liquid load in three structured packings. While effective area increased with liquid load, no dependence on viscosity was reported. However, surface tension has marginal impact on the effective mass transfer area. As has been noted elsewhere [12], however, an increase in liquid viscosity was achieved by an additive that simultaneously led to a significant decrease in surface tension. Janzen et al. [12] used X-ray computer tomography (XCT) to analyze the influence of viscosity and liquid load on both liquid hold-up and interfacial area in MellapakPlus 752.Y structured packing. Both hydrodynamic quantities were observed to increase with either increasing viscosity and/or liquid load.

Multiphase studies using the VOF method were focused on the wetting corrugated sheet, which was arranged similar to the packed column by Shojaee et al. [13] and Subramanian and Wozny [14]. Shojaee et al. [13] indirectly calculated interfacial area via the average value of film thickness and liquid

holdup in Gempak 2A packing. Furthermore, flow simulations were conducted in the representative elementary unit (REU) replicating identical hydrodynamics of the packing unit of structure packed column [15-18]. Ataki and Bart [19] conducted flow simulations in REU of Rombopack packing to study the impact of solvent properties on wetting, and also derived a correlation for the interfacial area. Haroun et al. [16] also used the VOF method to investigate the hydrodynamics in REU of Mellapak 250.X. The effects of solvent flow rate and contact angle on the interfacial area were investigated. Basden [15] also investigated the interfacial area and liquid holdup in the REU of packings. The effect of different parameters affecting hydrodynamics were studied. Sebastia-Saez et al. [17] also investigated a meso-scale model based on REUs of the MontzPak B1-250 packings to compute the interfacial area. Recently, multiphase flow investigations [18] in the REU of Gempak 3A were extensively conducted to develop correlation for interfacial area and liquid holdup in a packed column. The proposed correlations account for impacts of solvent properties, liquid load, and contact angle. Singh et al [20] continued further numerical studies to investigate the impact of prewetting and dynamic contact angle on the effective area in the REU of Mellapak 250.Y packing. The dynamic contact angle has a marginal effect on the interfacial area compared to the corresponding one predicted using static contact angle. However, the REU approach has some implication due to its small size and ability to feed the solvent from the top edge of sheet and have potential deviations in capturing the hydrodynamics at large industrial scale.

Wetting of columns is strongly connected to the packing surface behavior [21], including contact angle, surface texture, and sheet design. The contact angle is a property of solid-liquid systems in a specific environment [22] and a solvent contact angle varies based on the solid surface. A lower contact angle value promotes wetting, increasing the effective mass transfer area [23, 24]. Furthermore, surface texture or embossing increases wetting of the packed column [11, 25] by reducing the apparent contact angle [26, 27]. Recent studies of a rivulet falling over an inclined plate [24] and a single corrugated sheet [28] showed that the influence of contact angle on the surface area is linked to the surface tension of the solvent. The influence of the contact angle on the interfacial area [23, 24, 28] was found to more

significant for a solvent with a lower surface tension. The contact angle is difficult to measure since it is influenced by various factors such as packing material type, surface roughness, solvents, temperature, etc. [29]. Packing sheet of structured packed column may have been mechanically processed and have surface features on a micro and macro scales in the form of corrugation, bunches, and holes (Fig. 1). The surface texturing scatters the contact angle data in optically measurement with sessile droplets, [8]. Therefore, enhancing accuracy of the contact angle measurement is critical for predicting the effective mass transfer area thereby performance of packed columns for CO_2 capture. The effect of the packing geometry and features on wetting properties and, hence CO_2 capture efficiency, can be considered when estimating calculating effective contact angle.

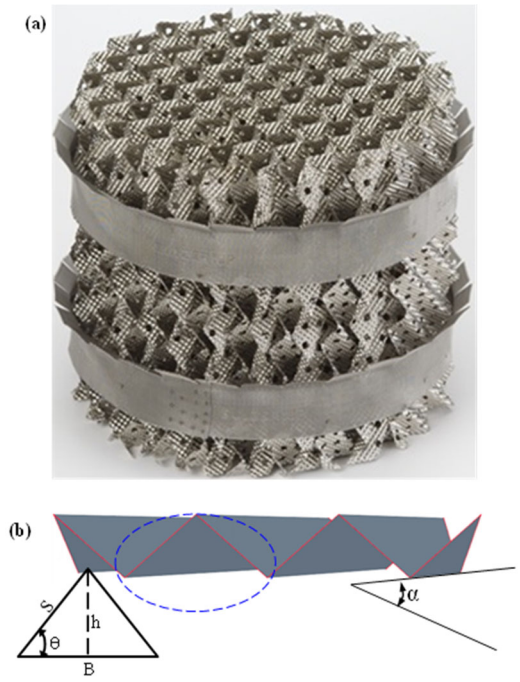

Fig. 1: (a) Photograph shows the design of a packing unit of Mellapak column built with perpendicular arrangement of corrugated sheets (source: https://www.sulzer.com). (b) Design of corrugated sheet to construct the computational model of packing unit of Mellapak packed column.

The wetting of the packing surface in the structure packed column is complex process that is still not fully understood at large scale, i.e industrial scale. Few attempts have been made to explain the local hydrodynamics in the packed column while taking into consideration all physical properties, temperature, CO_2 loading and packing surface characteristics. In this effort, multiscale simulation framework is

developed that is based on two-way coupling of CFD simulation for hydrodynamics with process modelling that incorporates reaction kinetics and thermodynamics in the commercial scale column.

This report presents the comprehensive unique multiscale approach to develop a surrogate model for effective mass transfer area in a structured packed columns for supporting pilot scale experiments. The effective contact angle on the packing surface, which describes the packing surface and solvent interaction, was measured using the modified Wilhelmy plate method accounting the physical properties of solvent, CO2 loading, and temperatures in Chapter 2. In Chapter 3, a comprehensive CFD simulation campaign based on the design of experiments were performed to derive a surrogate model of the effective mass transfer. The integration of developed algebraic surrogate model into the ASPEN PLUS process modelling is discussed in Chapter 4. In the last chapter, we conclude the summary of the work.

2. Contact angle measurement using modified Wilhelmy Plate method

The wetting behavior via solvent composition was performed by dynamic contact angle measurements of the tensiometer with the pre-determined surface tension correlation. The Mellapak sheet was selected for contact angle measurements. Contact angle was measured by submerging and withdrawing the Mellapak coupon in and out of the solvents. The wetting length of the coupon was calculated using corresponding 3D – XCT scanned images. The effective contact angle for a given pair of packing coupon and solvent were calculated using the coupon model, solvent properties and tensiometer force. The methodology, experimental setup, and contact angle measurement using the modified Wilhelmy plate method are extensively explained in the previous report [30], therefore brief overview are provided for the sake of brevity.

2.1 Wilhelmy plate method

The Wilhelmy plate technique [27], developed by Ludwig Wilhelmy, is used to measure surface tension and adhesion/cohesion for a particular surface and solvent pair using a tensiometer. This approach involves slowly immersing and retracting a coupon, whose weight is recorded using a microbalance, into and out of a solvent to allow wetting and direct measurement of surface tension and dynamic contact angle. The Wilhelmy plate method is based on force balance, which means balancing the interfacial tension force and gravity acting on a thin plate immersed vertically on the gas-liquid interface [28]. Measurement of coupon weight during the immersion stage enables for the deconvolution of the wetted force and buoyancy force imparted during wetting, which is correlated to the surface tension of the solvent, contact angle during wetting and the wetted lengths. Fig. 2 shows a perpendicularly submerged flat rectangular sheet in solvent. Using this process, first a flat platinum plate surface with assumed zero contact angle and complete wetting in the solvent to evaluate the surface tension of the solvent. The contact line perimeter of a rectangular plate (L) is calculated as $2(w+t)$, where w and t represent the width

and thickness of the plate, respectively. The surface tension force on the plate along the vertical direction $F_{\sigma,z}$ can be expressed as:

$$F_{\sigma,z} = \sigma L \cos\theta, \tag{1}$$

where, σ is the surface tension of the solvent and θ is the contact angle.

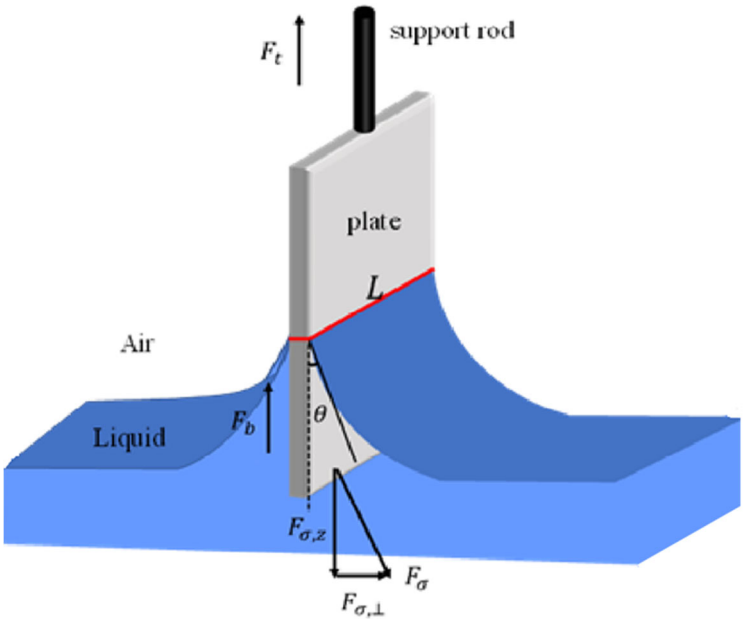

Fig. 2: Sketch describes the Wilhelmy plate method for contact angle (θ) and surface tension force ($\mathbf{F_\sigma}$) measurement. Coupon fabrication and surface characterization

The wetted perimeter and volume of the coupons are necessary for estimating the value of the effective contact angle. Mellapak coupon (shown in Fig. 3 (a&b)) was selected to represent the packing materials used in the structured packed columns. Sheet stocks in 316 SS were purchased from packing manufacturer to prepare the packing coupons: the Mellapak is from Sulzer Chemtech, USA. Rectangular coupons with dimension of 2 cm x 2 cm were wire cut from the Mellapak sheet using electric discharge machining (EDM). For immersion and pulling of the coupon sample, a 4 cm 304 SS wire rod with a 1.145 mm diameter was spot welded to each coupon.

The coupon specimen was imaged using a high-resolution ZEISS Versa 610 X-Ray microscope with a spatial resolution of 500 nm (Fig. 3). Stacks of 2D slices of the scanned images were exported as digital image files for 3D geometry reconstruction. Using the in-house MATLAB® code, images were

postprocessed to extract the volume and wetted perimeter in the direction parallel to the attached rod. The computed tomography (CT) image, sliced in the x-y plane, has an isotropic resolution of 0.02 mm per pixel. Each coupon sample consists of 1018 two-dimensional slices, each with a resolution of 1024 × 1024 pixels. The larger surface feature (> 0.10 mm) of coupons is fully resolved by XCT while retaining all of the geometry's finer details.

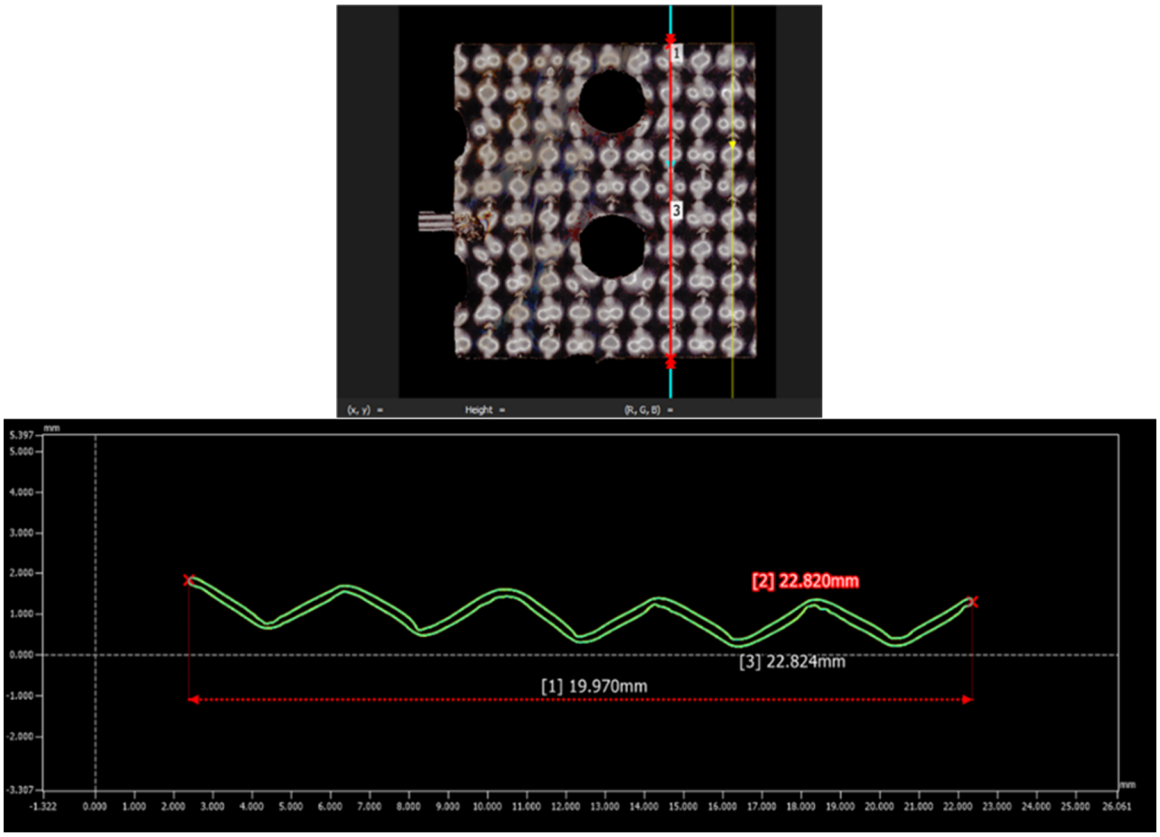

Fig. 3: (a) Scanned image of the Mellapak coupon. (b) Length of perimeter at a specific vertical z-position denoted by the red line in Figure (a).

Detailed methodology and steps for the image reconstruction from the XCT image to the computer-aided design (CAD) model has been extensively explained in the previous report [31]. The coupon has a nominal height of 20 mm and a width of 20 mm. A SS rod has been welded at the top of the coupon to facilitate the conducted dynamic contact angle measurements. The perimeter profile along the z-direction can be obtained using the reconstructed 3D geometry. The surface normal of the coupon

undergoes a significant directional change in the vicinity of the hole. The average coupon perimeter is approximately 45.13 mm, and a width of 22.41 mm.

2.2 Experiment Design and Description

Experimental setup and protocol for the calculation of effective contact angle are extensively explained in the previous reports [30, 31]. For sake of brevity, experimental design and measurement are briefly described here. The experimental setup was designed and fabricated to investigate the effects of various factors such as packing surface design, physical properties of solvent, temperature, CO_2 loading, and contact line movement on the contact angle. The experiment was focused to evaluate Mellapak packing surface structures using aqueous solvent of 30% MEA by weight (30% MEA), NaOH and EEMPA at different temperatures. The experimental investigations were performed to evaluate the operation of a CO_2 capture process, i.e. CO_2 loading on effective contact angle for EEMPA solvent.

As shown in Equation (1), tensiometer force $F_t\ (z)$ is required to measure surface tension force $F_{\sigma,z}$ and the effective contact angle for a given solvent and solid substrate combination. The surface tension and liquid density of solvent were measured using a KRÜSS tensiometer K100C (KRÜSS GmbH, Hamburg, Germany). Fig. 4 shows that, the tensiometer is connected to a recirculatory bath (NESLAB, Ex-111), a custom gas manifold, and computer for the data acquisition. The temperature of the solvent was regulated controlled using control jacket, which is plumbed to the recirculatory bath. To control the gas concentrations within the sample chamber, the gas supply and vent lines are connected to the back of the tensiometer. CO_2 and nitrogen (N_2) gases are introduced into the system through an externally plumbed manifold system.

Before measuring surface tension of solvent, the Wilhelmy plate was cleaned with organic solvent and deionized water. The coupon sample was then burned to a red-hot temperature to eliminate any impurities sticking to its surface. A desired amount of CO_2 is dissolved into the solvent using a specially built volumetric equipment. The lean and rich solvent compositions estimated during continuous

capture process are used to determine CO_2 loadings. To prepare the desired CO_2 loading for the EEMPA testing solvent, dry ice was introduced. Initially, the EEMPA solvent was mixed with deionized water. The mixture was stirred using a magnetic stirrer bar in the glass vessel. The dry ice pellets were gradually added into the solvent until the increased mass reaches to the desired CO_2 loading. It is important to note that majority the dry ice sublimated, and only the mass of the CO_2 that reacted with the solvent was evaluated. The loaded solvent was mixed using the magnetic stirrer bar and left undisturbed for 1 - 2 hours until it achieves equilibrium conditions.

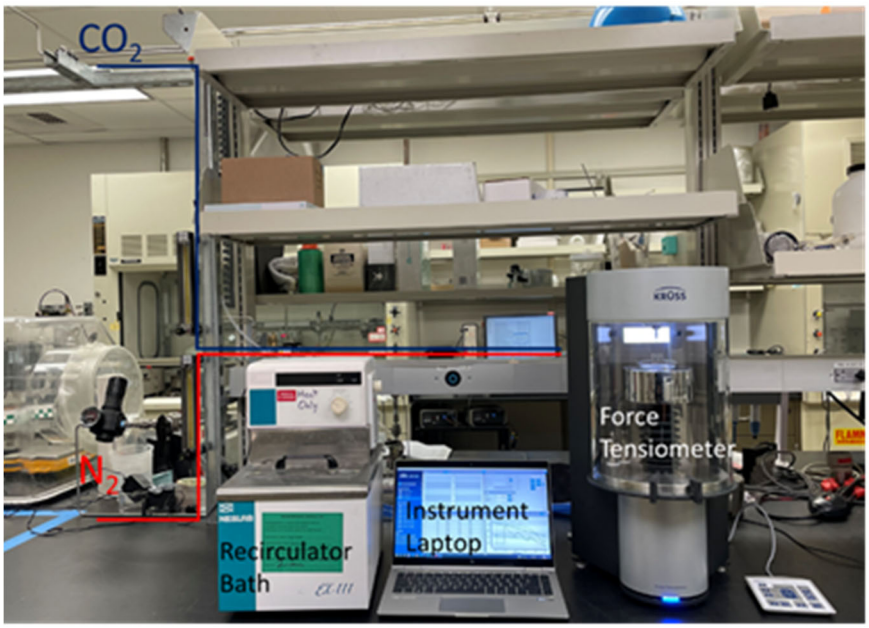

Fig. 4: Experimental setup including the KRÜSS K100C and its associated setup, a recirculatory bath, gas manifold, and instrument laptop. Surface tension measurement using the Wilhelmy plate method with the gas flow through the gas enclosure

The advanced software supplied with the tensiometer includes modules for measuring surface tension using the Wilhelmy technique, solvent density, and dynamic contact angle, etc.

2.3 Effective contact angle for the Mellapak Coupon

As explained earlier [30], the surface tension value of the 0.10 M aqueous NaOH solvent was modified with surfactant. The Mellapak coupon was first tested at temperature of 25 ºC with three solvents i.e.

aqueous NaOH, aqueous MEA and water-lean solvent EEMPA. As shown in Fig. 5, the value of effective contact does not change significantly with the variation of surface tension value of all solvents. The effective contact angle remains nearly constant due to surface texture and perforation holes of Mellapak sheet. Next, aforementioned solvents and aqueous NaOH with varied surfactant concentrations were tested on the Mellapak coupon (Fig. 5). The coupon showed marginal impact on contact angle regardless of solvent surface tension value. This observation is counterintuitive to literature for contact angle measurements (performed on a goniometer) on smooth and flat surfaces, which demonstrated a direct correlation with surface tension of solvent. The disparity between the present observation and previous literature was due to (1) the lack of surface textures in previous experiments (2) the dry surface condition sample during experiments, and (3) the methodology for measuring contact angles (static versus dynamic). The same experiments were repeated for dry coupon, and the observed results revealed the impact as a function of surface tension value. However, this impact was observed to be marginal. This observation showed that the surface textures play a dominant role in decreasing the contribution of surface tension to wetting behavior. To verify this uniquely observed behavior, control tests were performed in the same protocol with a flat smooth coupon of the same material composition without any surface features/textures. In this case, a higher surface tension solvents showed larger contact angles. This verifies the assumption that the surface textures of representative packing material of Mellapak 250.Y have no substantial impact surface tension on contact angle. Indeed, the influence of surface texture on wetting of flat sheet was investigated by Iso and Chen [32], and found that the lateral texture improves the sheet wetting. Further, contact angle was also calculated for different CO_2 and water loadings on EEMPA. The water loaded EEMPS shows the slightly lower value of the contact angle whereas the CO2 loaded solvent shows higher value of contact angle. However, all solvents show approximately constant value of the contact angle. This measured value of the contact angle will be further used for interfacial area prediction in CFD simulations.

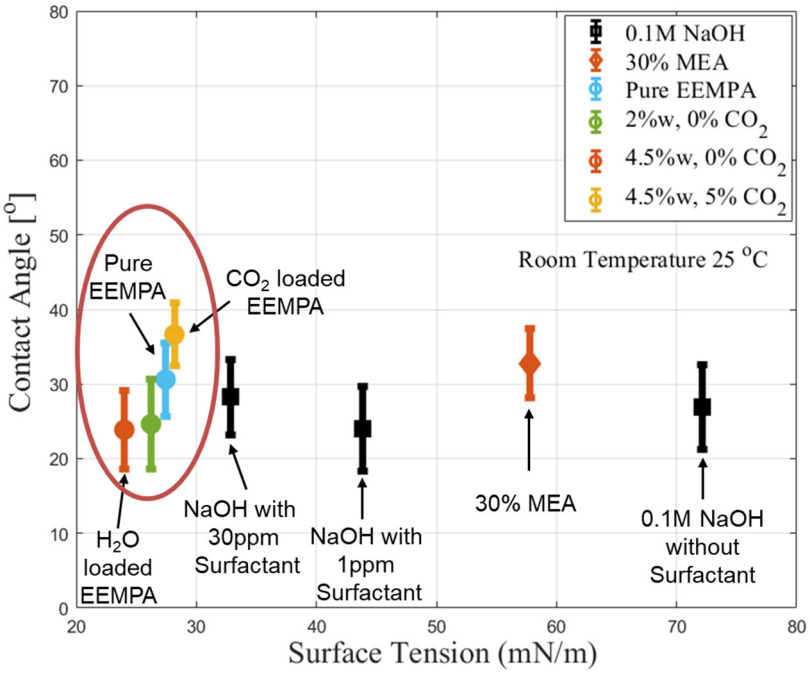

Fig. 5: Effective contact angle distribution for the Mellapak coupon at 25 °C for different solvents.

2.4 Effect of temperature on contact angle

The corrected surface tension force for the Mellapak coupons were calculated first and contact angles were calculated using the intersection method. It should be noted that a packed column exhibits different temperatures at depending on the inlet flue gas temperature as well as packing stages. Indeed, temperature varies axially along the height of the packed column, thereby packing stages has different temperature in the column. Because physical properties of solvent vary with temperature, variation in the value of contact angle is expected. Accordingly, the contact angle of the EEMPA solvent for the Mellapak coupon was examined at three temperatures (25 ºC, 40 ºC, and 60 ºC). In Fig. 6, it can be observed that the contact angle increases with increased surface tension value. Further, contact angle decreases with increasing temperature value. This is somewhat expected given that surface tension of solvent decreases as solvent temperature increases. Next, regression analyses were performed to derive a correlation for the variation of the contact angle with solvent temperature (Fig. 6). This correlation will be employed in the surrogate modeling for interfacial area and computation of the interfacial area in process modelling at different stages of column packing in pilot scale testing.

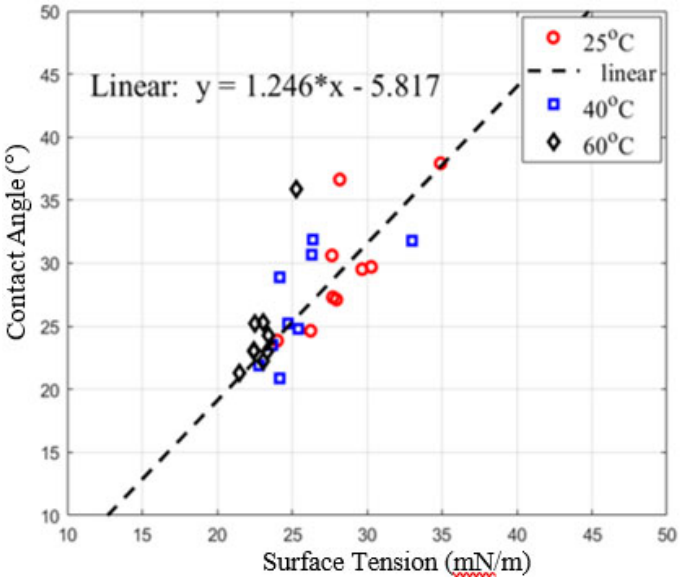

Fig. 6: Variation of the contact angle with surface tension of EEMPA at different temperatures. Fitting of contact angle with surface tension shows a linear fitting at temperature included.

3. Computational Modeling

3.1 Mathematical formulations

Multiphase flow simulations were conducted using STAR-CCM+ [33] to investigate the hydrodynamics of the Mellapak 250.Y structure packed column. The VOF method [34] is chosen in the multiphase flow simulations, which is based on a single-fluid formulation and suitable for the stratified flow studies. The governing equations are as follows:

$$\nabla \cdot \mathbf{u} = 0, \tag{2}$$

$$\frac{\partial(\rho \mathbf{u})}{\partial t} + \nabla \cdot (\rho \mathbf{u}\mathbf{u}) = -\nabla p + \mu \nabla \cdot \left[\nabla \mathbf{u} + (\nabla \mathbf{u})^T \right] + \rho \mathbf{g} + \nabla \cdot \left(-\overline{\rho \mathbf{u}'\mathbf{u}'} \right) + \mathbf{F}, \tag{3}$$

Here, **u** is the velocity, p is the pressure, **g** is the gravity, and **F** is the interfacial tension force. The terms ρ and μ are phase averaged value of density and viscosity, respectively. The term $-\overline{\rho \mathbf{u}'\mathbf{u}'}$ in Equation (2) is the Reynolds stresses and Boussinesq hypothesis [35] was used to correlate the Reynolds stresses to the mean velocity gradient:

$$-\overline{\rho \mathbf{u}'\mathbf{u}'} = \boldsymbol{\tau} = 2\mu_t \mathbf{S} - \frac{2}{3}\rho k \mathbf{I} \tag{4}$$

where, μ_t is the turbulent viscosity, k is the turbulent kinetic energy, $\mathbf{I}$ is the identity tensor, and **S** is the strain rate tensor defined as: $\mathbf{S} = \frac{1}{2}\left[\nabla \mathbf{u} + (\nabla \mathbf{u})^{\mathrm{T}} \right]$.

The continuous surface force method [36] was used to calculate **F** at the gas-liquid interface:

$$\mathbf{F} = \sigma \frac{\rho \kappa \nabla \alpha}{\frac{1}{2}(\rho_l + \rho_g)} \tag{5}$$

where, σ is the surface tension, α is the volume fraction of the primary phase that varies from 0 to 1, and ∇α represents the direction vector at the interface. Subscripts l and g denote the liquid and gas phases respectively. The curvature κ is the local curvature of the interface, which is computed as the divergence of the unit normal ($\mathbf{n} = \nabla\alpha/|\nabla\alpha|$):

$$\kappa = \nabla \cdot \mathbf{n} \tag{6}$$

The interface between the phases is captured by solving the transport equation of volume fraction.

$$\frac{\partial \alpha}{\partial t} + \nabla \cdot \left(\mathbf{u}\, \alpha \right) + \nabla \cdot \left(\mathbf{u}_{\mathbf{c}} \alpha (1 - \alpha) \right) = 0 \tag{7}$$

The last term in the left side of the equation (7) functions only proximately to the gas-liquid interface to prevent the interface smearing. $\mathbf{u_c}$ $\left(= C_\alpha \times |\mathbf{u}| \frac{\nabla \alpha}{|\nabla \alpha|} \right)$ is the sharpening velocity, and C_α is sharpening factor.

3.2 Turbulence Modeling

The flow in the packed column is considered to be turbulent because of its complex geometry, and chaotic flows departing from the Darcy flows [37, 38]. For additional closures of turbulence, the two-equation Shear Stress Transport (SST) $k - \omega$ turbulence model [39] is used, which is appropriate for modeling turbulent flow in the packed columns [40-44]. The following are transport equations for the SST $k - \omega$ turbulence model:

$$\frac{\partial (\rho k)}{\partial t} + \nabla \cdot \left(\rho \mathbf{u} k \right) = P + \nabla \cdot \left[\left(\mu + \sigma_k \mu_t \right) \nabla k \right] - \rho \beta^* \omega k + S_k \tag{8}$$

$$\frac{\partial (\rho \omega)}{\partial t} + \nabla \cdot \left(\rho \mathbf{u} \omega \right) = \frac{\rho \gamma}{\mu_t} P - \rho \beta f_\beta \omega^2 + \nabla \cdot \left[\left(\mu + \sigma_\omega \mu_t \right) \nabla \omega \right] + S_\omega \tag{9}$$

where, ω is turbulent dissipation rate per unit turbulent kinetic energy ($\omega = \epsilon / k$). P is the production limiter that is calculated as follows:

$$P = \min \left(P_k,\ 10 \rho \beta_0^* k \omega \right) \tag{10}$$

P_k is the production rate of the turbulent kinetic energy due to the mean velocity gradient and is calculated as:

$$P_k = \boldsymbol{\tau} : \nabla \mathbf{u} \tag{11}$$

α_k and α_ε are the inverse of effective turbulent Prandtl numbers for the k and ω equations, respectively. The eddy viscosity (μ_t) is computed as:

$$\mu_t = \frac{\rho a_1 k}{\max \left(a_1 \omega, \mathrm{S} F_2 \right)} \tag{12}$$

where, S is the magnitude of strain rate tensor computed as $S = \sqrt{2\mathbf{S}:\mathbf{S}}$. The value of empirical constants used in the equations (7 – 11) used are values specified by Menter [39].

3.3 Solution Scheme

The transient multiphase flow simulations were carried out using the implicit time integration scheme that comprises several inner iterations in a single time step to achieve convergence. The segregated solver was used in the flow simulations that uses the pressure-velocity coupling method to satisfy continuity by solving the pressure correction equation. The pressure-velocity coupling was achieved by using a predictor-corrector approach using the SIMPLE algorithm [56]. The second-order upwind scheme was used in the spatial discretization of all equations. The simulations use an algebraic multigrid method (AMG) linear solver with Gauss-Seidel relaxation scheme for faster convergence of each transport equation. High-resolution interface capturing (HRIC) with the capability of capturing sharp interfaces is used in the convection scheme of the transport equation of volume fraction [57]. The flow simulations required very small time step ($\Delta t \sim 10^{-5} - 10^{-4}$sec) to satisfy the Courant–Friedrichs–Levy (CFL) conditions according to value of the Courant number as 0.50 for the stable and converged simulation.

3.4 Design of experiments (DOE)

As mentioned earlier, prediction of the effective mass transfer area in the structure is complex quantity because it depends on various factors such gas load, liquid load, contact angle, physical properties, contact angle, etc. To understand the impact of these various factors, design of experiments (DoE) was employed. DoE strategy enables adaptive learning based on results outcome while simulation is being run. DoE model enables to include the strategy to design the simulation campaign with greater flexibility, allowing for the selection of the most relevant parameters.

The input parameters potentially affecting the interfacial area, namely solvent velocity u_L representative as liquid load ($q_L = 3600u_L\ m^3/m^2h$), gas velocity u_G, representative of gas load ($F_G = u_G\sqrt{\rho_G}$), contact angle θ, solvent viscosity μ_L and surface tension σ, and solvent density ρ_L, are

selected in DoE to compute the individual impact on the interfacial area in the structured packed column. The range of parameters used in the DoE are presented in Table 1.

Table 1: Range of parameters used in the DoE for CFD simulation campaign.

Parameters	**Unit**	**Range**
Solvent velocity (u_L)	*m/s*	0.0008 – 0.028
Gas velocity (u_G)	*m/s*	0.36 – 2.20
Solvent viscosity (ρ_L)	*Pa·s*	0.0005 -0.05
Solvent density (ρ_L)	kg/m^3	940 - 1050
Surface tension (σ)	*N/m*	0.01 - 0.10
Contact angle (θ)	^{o}	2 - 90

DoE systematically examines the significant impact of the six input parameters in the sample shown in Table 1 using Latin Hypercube Sampling (LHS) [33]. LHS is a widely used approach for generating controlled random samples that is more efficient than the standard Monte Carlo method. In the LHS, each input parameter is grouped into *N* equal strata and parameter is sampled once in each stratum. The aforementioned six input parameters are then randomly combined using the generated LHS samples. The LHS covers the space of each input parameter uniformly without increasing the number of designed sets. A total number of 300 CFD simulation runs were designed for countercurrent flow in the structured packing unit. The detail of the design is ploFig. tted in Fig. 7. These ranges of the physical properties cover the solvents such as aqueous solvent, such as Sodium Hydroxide (NaOH) [34], aqueous Monoethanolamine (MEA) [35]–[38] as well as water lean CO_2-Binding-Organic-Liquids (CO_2BOL) solvent [18], [39], [40], commonly used for CO_2 capture process.

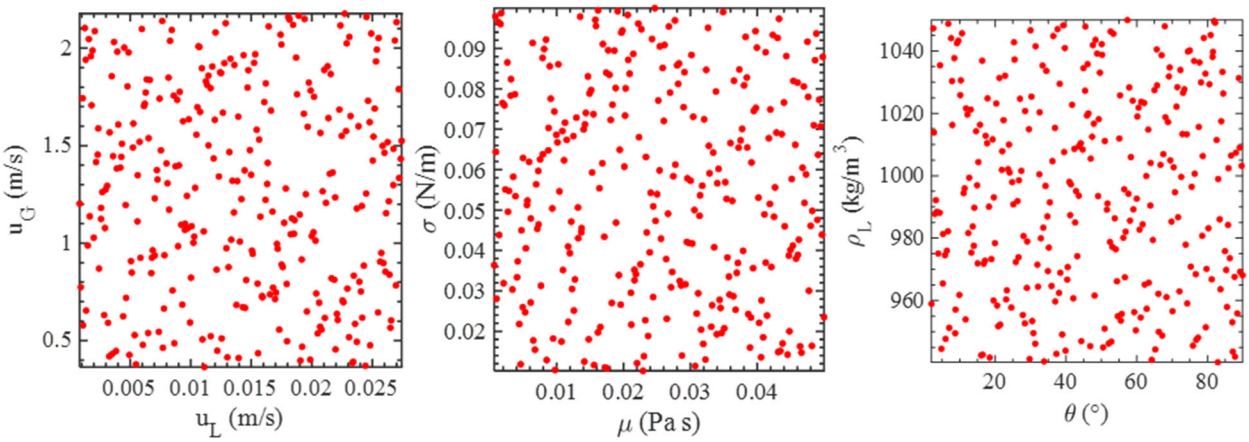

Fig. 7: Visualization of input parameter distributions sampled with Latin hypercube method.

3.5 Parameter sensitivity analysis

The sensitivity score is computed using the fitted MARS model [45]. Method for the computation of sensitivity score for different parameters influencing the effective mass transfer area are extensively presented in our previous work [46]. Therefore, it is not explained here for the sake of brevity. Fig. 8 shows the relative significance of the included input parameters based on the computed sensitivity scores. The figure shows solvent velocity, surface tension, gas velocity and contact angle as the most influential parameters impacting the interfacial area. They account for nearly 99% of the variability in the interfacial area prediction. The solvent viscosity and density have the least effect on the interfacial area in the structured packed columns. The ranking of these input parameters in the Pareto plot informs the selection of the input parameters for the development of surrogate model for interfacial area. As seen in the Fig. 8, variation of the solvent density has the least impact, therefore, it was not included in the surrogate model development.

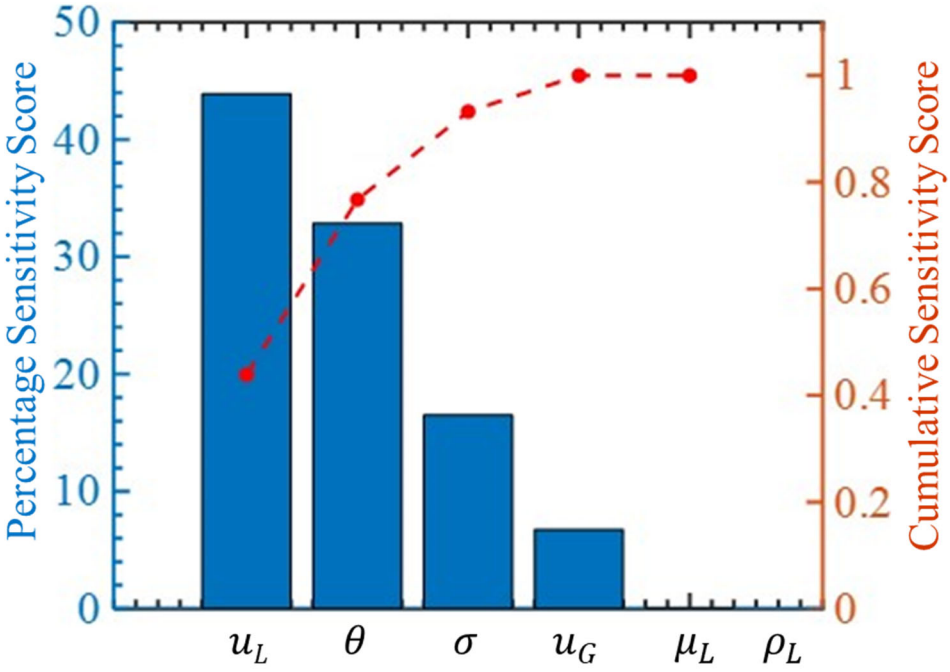

Fig. 8: Pareto plots show the influence of $u_L, u_G, \theta, \sigma, \mu_L$ and ρ_L on the interfacial area in the structured packed column.

4. CFD simulations and Surrogate model

4.1 Computational domain and Meshing

We perform flow simulations for calculating effective mass transfer area in the Sulzer Mellapak 250.Y packing (Fig. 1). Similar to the previous studies [15, 18, 42], a model of the computational flow domain was created by perpendicular arrangement of two corrugated sheets. It consists of three units in both lateral and flow directions (see Fig. 9 (a)). A 2mm gap was provided between sheets according to industrial design. Design of the corrugated sheet is the same as the standard design of Mellapak 250.Y (see Fig. 1 (b) and Table 2), and perforation was excluded in the flow simulation. Previous studies by Green et al. [47] suggested that liquid films cover holes for the majority of the operated liquid loads, and, eventually, it leads to minimal area loss. Therefore, results for sheets without perforation would not be significantly different from perforated ones. A schematic of the computational flow domain is presented in Fig. 9(a). The computational flow domains were extended at bottom and top as well. The top extended section includes liquid distributor that contains 64 dripping points that have diameter of 4 mm and 15 mm. The bottom extension aid in specification of boundary conditions for smooth convergence and stable simulations. Furthermore, simulation results in the packed column will only be assessed in the region consisting of packing sheet.

Table 2: Design of the corrugated sheet used in packing unit Mellapak 250.Y packing.

Parameters	**Dimension**
Corrugation angle (α)	45°
Channel base (B)	26.70 mm
Channel height (h)	12.00 mm
Channel side (s)	17.00 mm
Specific Area (a_p)	250 m^2/m^3

Due to the complex model of the packed column and complex flow regime (in particular, corrugated sheets comprised of inclined triangular channels) modeling the computational flow domain is challenging. The model of flow domain was created in the STAR-CCM+ using the dimensions provided in Table 2 (see Fig. 9 (a)). Meshing of the domain, one of the crucial steps affecting stability and accuracy

of the results, was also performed in STAR-CCM+. To capture hydrodynamics of the countercurrent flow accurately and efficiently, flow domain was discretized with nonuniform mesh. As shown meshing of flow domain in Fig. 9(b), the mesh near the sheets was generated using prism layer meshing (similar as boundary layer mesh) scheme. Liquid film appears near the wall therefore, it requires very fine mesh. Inflexion regions of the triangular channels were also refined to capture the hydrodynamics. Further, the gradient based polyhedral mesh was used to discretize the reaming region of the flow domain. Subsequently, the size of mesh proximate to the prizm layer is smaller than the mesh in the center of domain (see in Fig. 9(b)). Note the center of domain does not actively contribute to transport phenomenon of interest. Subsequently, 2.0 million cells in the flow domain were obtained after grid convergence tests.

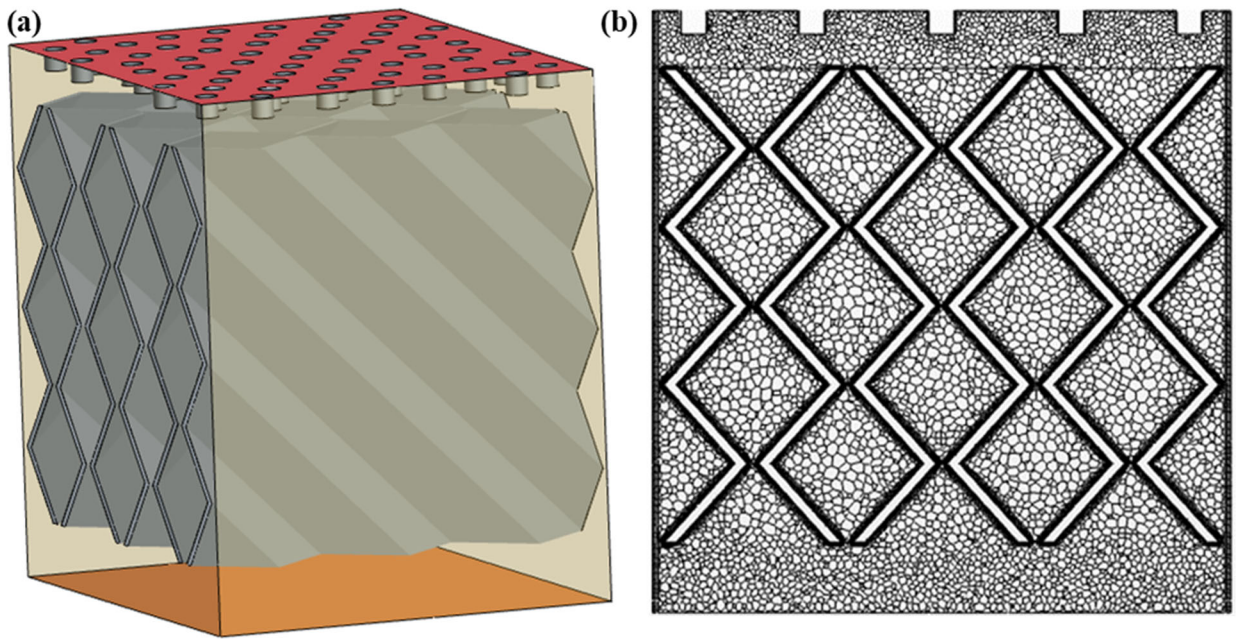

Fig. 9: (a) 3D view of the computational flow domain of REU shows the countercurrent flow direction of gas and solvents. The periodic boundary (depicted in light yellow color) is specified along all vertical sides of the domain. Liquid is fed via dripping points (tiny cylinders) from the top and gas was injected from the bottom of flow domain. (b) Meshing of the flow domain shows the polyhedral cells used in flow domain and very fine mesh near the sheet (appearing black dark lines due to high mesh density) where gas-liquid interface is expected to exist

The solvent enters in the flow domain via dripping points and exits from the bottom due to gravity (see orange colored rectangular plane in Fig. 9(a)). In the simulation, the sheet was set as no-slip walls with the specified contact angle measured using the modified Wilhelmy plate method. All four

vertical sides of the flow domain were specified as periodic boundary that allow flow to cross and reenter in the flow domain through lateral boundaries (side walls). The bottom of the flow domain was set to pressure outlet boundary with atmospheric condition. The uniform inlet velocity was specified at the solvent inlet at the dripping points at the flow domain. Positive (solvent inlet at dripping point) and negative (gas at the top) values of the velocity were specified to impose countercurrent flows. Similar boundary conditions for liquid and gas inlets were previously used in such flow simulations [13, 16, 20, 48].

Flow simulations were terminated when the normalized interfacial area in the column reaches pseudo-steady state (see Fig. 10 (b)). The results were then further investigated, and a surrogate model for interfacial area was developed. Time required to achieve the pseudo-steady state depends on solvent properties, contact angle, gas, and liquid loads, etc., and vary case by case. The time to achieve pseudo-steady takes at least 3-4 seconds (Fig. 10 (b)). Subsequently, flow simulations were expensive, e.g., a single simulation takes couple of days of wall clock time using 192 cores on Pacific Northwest National Laboratory (PNNL) supercomputers.

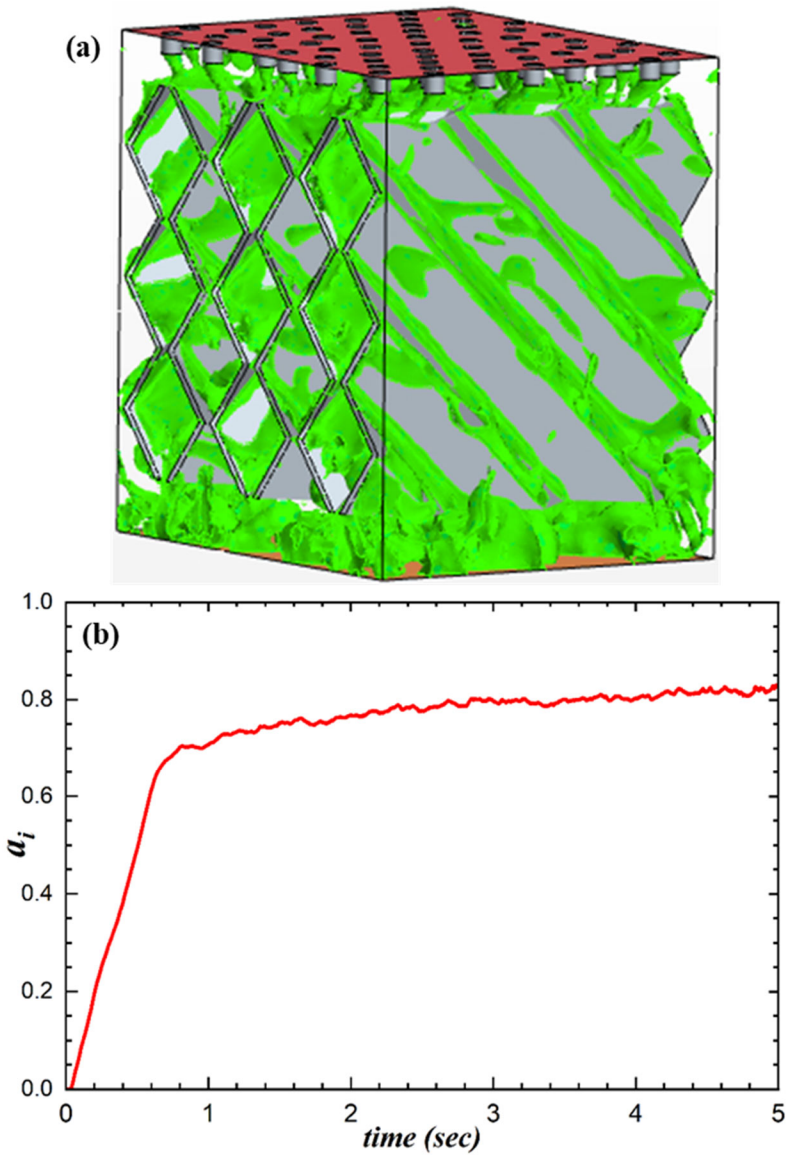

Fig. 10: (a) Snapshot for the evolution of interface in structured packed column. (b) Temporal evolution of the normalized interfacial area (a_i) in structured packed column. the pseudo-steady state is considered when value of the normalized interfacial area becomes nearly constant.

4.2 Comparison of CFD predicted interfacial area with experiments.

Preliminary flow simulations were carried out to validate CFD prediction, demonstrating reliability and accuracy of the flow prediction. Accordingly, predicted effective area are compared to experimental data to validate the VOF simulation framework for computation of effective area in Mellapak 250.Y packing [9]. Tsai et al. [9] measured the effective mass transfer area of Mellapak 250.Y packing having 0.46 m and 0.427 m outer and inner diameters, respectively. 0.1M aqueous solution of

NaOH was used as solvent. Air was introduced from the bottom of the packing and air velocity was in the range of 0.50–1.50 m/s.

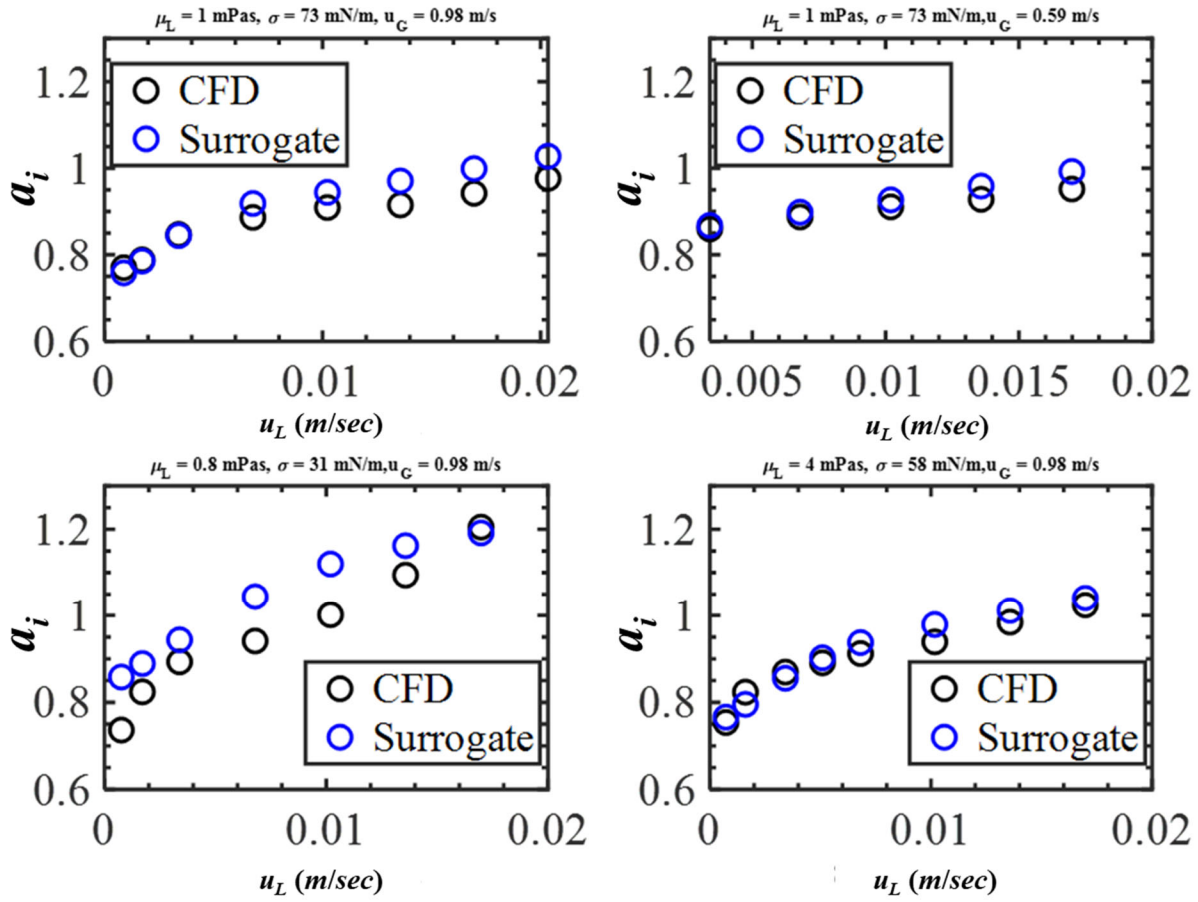

Fig. 11: Comparison of the predicted effective area with experimental data by Tsai et al. [8] at different solvent velocity, u_L (liquid loads).

The predicted effective area was computed for different values of surface tension, solvent velocities, viscosity and two gas velocities. Fig. 11 shows the comparison between CFD predicted effective area and the experiments. As expected, effective area increases as liquid loads increase for both methods for all cases. The predicted effective area (a_i) matches well with the experimental data for all cases. A discrepancy is found at higher velocity for case with high surface tension value; otherwise, both show good matching.

Over the last decade in CCSI, we have reported a series of validation efforts for prediction of free surface flows (rivulet, film flow, droplet) against corresponding experimental results in various

configurations (i.e. bottom up approach) of packed column using VOF method [20, 24, 28, 48-51]. For a film over a smooth inclined plate [24], predicted wetted area and film thickness using VOF method were found to match well with the experimental results of Hoffmann et al [52] and Nusselt theory [53], respectively. VOF simulations for rivulet falling over an inclined plate were also validated against in-house experiment at PNNL for water and silicon oil [50]. The predicted braiding and meandering instabilities in the water rivulet were observed to be consistent with experiments. Subsequently, the wetting of a corrugated sheet of Montz packing matched qualitatively well with experiments of Subramanian and Wozny [14] for three solvents [28]. Recently, validation of multiphase flow simulations for a 3D printed Schwarz packed columns was extensively reported [48]. It would be worth noting that the VOF method has been successfully used in similar flow studies by many researchers for reactive mass transfer in a two-phase flow system [54-57]. Therefore, it can be concluded that the VOF method is an appropriate method to investigate the hydrodynamics and effective mass transfer area in structured packed column.

4.3 Development of Surrogate model

The surrogate model for the effective area was developed using FOQUS [58], a computational framework developed under CCSI for Optimization and Quantification of Uncertainty and Sensitivity. To develop a surrogate model for predicting interface area with the input information of solvent flow rate, gas flow rate, surface tension, contact angle, and liquid viscosity was selected. These five quantities were selected based on the outcome of sensitivity analyses. The surrogate model can be integrated into Aspen+ model directly as a .dll FORTRAN subroutine. As mentioned earlier, a comprehensive and extensive CFD simulations campaign was performed to predict the interface area under different combinations of the five factors (solvent flow rate u_L, gas flow rate u_G, surface tension σ, contact angle θ, and liquid viscosity μ_L), as shown in Fig. 12.

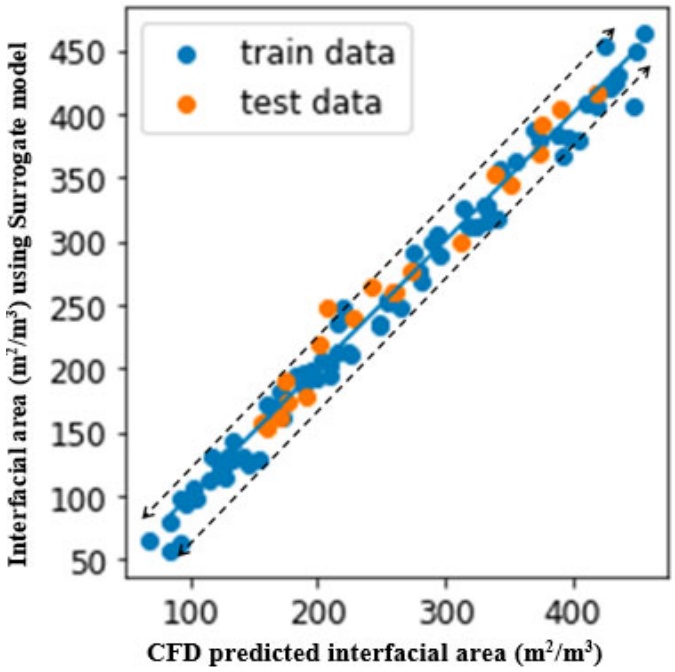

Fig. 12: Parity scatter plot for training accuracy vs testing accuracy of the surrogate model for interface area prediction.

The obtained CFD data for interfacial area is then fitted with a proper fitting function to reproduce interface area's dependency on the five factors: specific area $a_i = f(u_L, u_G, \sigma, \theta, \mu_L)$. 80% CFD data (shown by blue circle) is used to train the surrogate model, while 20% (depicted by the brown circle) is used to test its reliability when applied to new cases, as seen in Fig. 13.

Design	uL [m/s]	uG [m/s]	Viscosity mu_L [Pa	Surface tension sigma [N/m]	Contact Anlge CA	CFD_ai [m2/m3]
1	1.49E-03	1.175499094	0.023401693	0.098583453	71.09	0.55
2	1.01E-02	1.488005879	0.013453918	0.079459361	16.33	0.92
3	2.20E-02	1.38232513	0.025884167	0.077178727	44.6	0.9
4	9.46E-03	1.005498878	0.039589923	0.011489487	78.61	1.37
5	4.92E-03	1.363206582	0.009560703	0.076335761	77.2	0.79
6	2.26E-02	1.790884988	0.024900201	0.035950652	63.61	1.03
7	1.34E-03	0.970302457	0.038253195	0.032198636	66.63	0.63
8	1.89E-02	2.070127827	0.038923688	0.034575202	83.44	0.93
9	0.021223146	1.717312085	0.014634644	0.078037645	15.09	0.97
10	0.0235512	1.342458728	0.003567398	0.031247034	28.78	1.13
11	0.016253773	0.987020456	0.047013131	0.022689393	61.16	1.17
12	0.025318521	1.824955495	0.03548356	0.056044129	20.31	1.03
13	0.011568695	2.097521204	0.042916848	0.050242369	56.8	0.87
14	0.00928497	1.356676465	0.026376328	0.02811221	20.94	1.05

Fig. 13: Snapshot of the CFD database for interface area prediction based on five variables.

4.4 Comparison of surrogated and CFD predicted interfacial area

After development of the surrogate model, the interfacial area at the same condition (presented in Fig. 11)was calculated. The interfacial area obtained from the surrogate model was further compared with CFD predicted value in Fig. 14. A good agreement between both values of the interfacial is found at a range of solvent velocity.

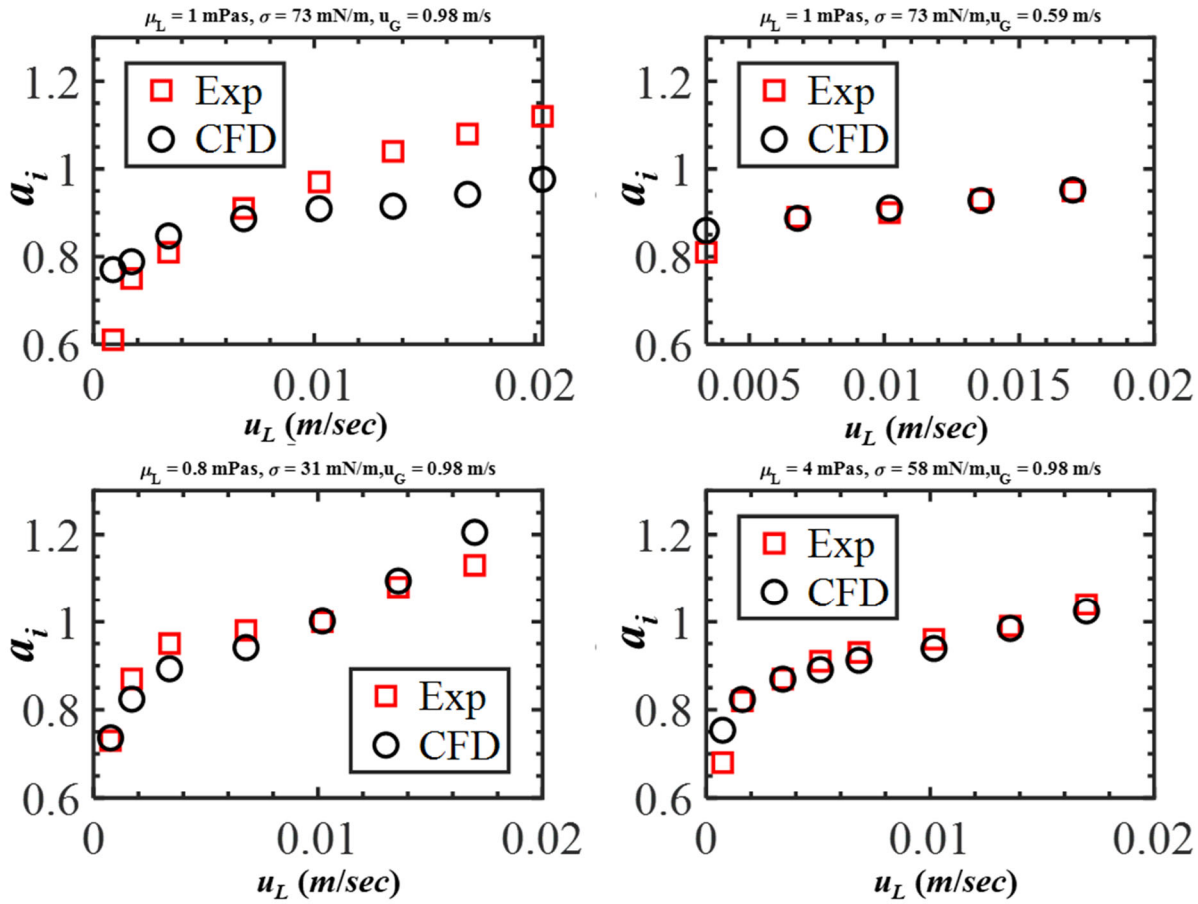

Fig. 14: Comparison of the predicted effective area using CFD simulations with corresponding one from surrogate model at different solvent velocities, u_L (liquid loads).

4.5 Uncertainty in surrogate model

The uncertainty of the surrogate model mainly comes from two aspects. One is the fitting error of the surrogate model itself when fitting to CFD data. It shows the surrogate model's fitting error follows Gaussian distribution, and thus we can theoretically evaluate the potential uncertainty of the surrogate model and the confidence interval of interface area based on the normal distribution theory, as shown in

Fig. 3. Based on the fitting condition, we get that the 95% confidence interval of discrepancy of the predicted specific area is [-0.06, 0.06]. That is, we are 95% confident that the actual specific area is within [a_i-0.06, a_i+0.06], where a_i is the specific area predicted by the surrogate model.

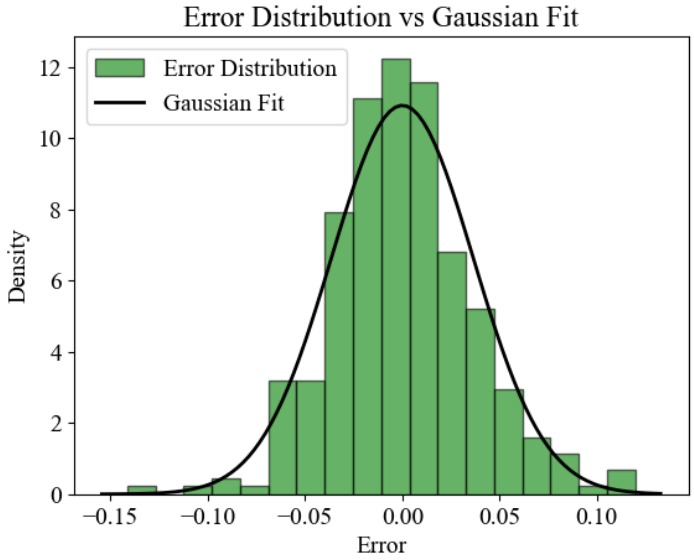

Fig. 15: Fitting error of surrogate model follows the Gaussian distribution.

Another is the uncertainty of contact angle. Since Aspen+ model does not calculate contact angle explicitly, the contact angle is determined based on a correlation where contact angle is a function of surface tension only, as shown earlier in Fig. 6. The correlation equation has errors when fitting to experiment data, which may cause the uncertainty of contact angle calculations.

4.6 Integration of surrogate model in ASPEN Plus

The subroutine predicts the interfacial area using the surrogate model with the inputs of flow rate of solvent and gas, surface tension, and liquid viscosity, as well as two user-specified parameters δ_1, δ_2. The first parameter δ_1 specifies the correction term added to contact angle. The contact angle is calculated using the correlation of the contact angle with contact angle in Fig. 6 as θ_0, then the user-specified contact angle will be modified as $\theta = \theta_0 + \delta_1$. The second parameter δ_2 specifies the correction term added to specific area considering to the fitting error. The final specific area will be $a_i + \delta_2$, where a_i is the specific area predicted by the surrogate model.

The final specific area = $f(u_L, u, \sigma, \theta_0 + \delta_1, \mu_L) + \delta_2$.

Eventually, the specific area will be converted to interface area when interfacing with Aspen+.

To use the subroutine of surrogate model for interface area calculation, choose 'INTFAML' in the Name box, as shown in Fig. 16. Note that, two associated real parameters should be specified as a part of inputs of the subroutine. The first one corresponds to δ_1 while the second one to δ_2.

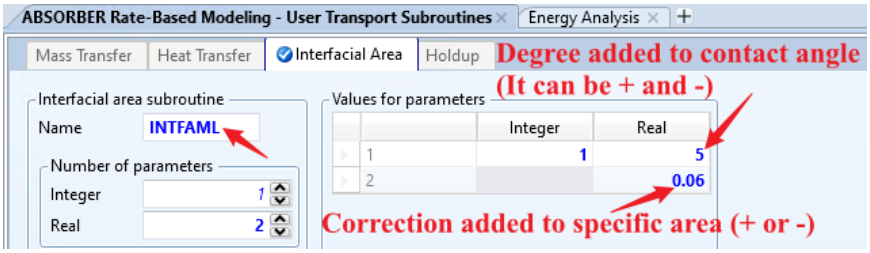

Fig. 16: Snapshot of interface area setup in Aspen Plus.

5. Conclusion

The post-combustion carbon capture via solvent absorption in a packed column has gained widespread interest because of its potential applications in the mitigation of CO_2 emissions from fossil fueled power plants. CFD modeling of solvent absorption in structured packed column is a multi-scale problem due to wide range of length scale. It is worth noting that the local hydrodynamics plays a critical role is determining the overall column efficiency.

The interfacial area, also referred as effective mass transfer area, is an important parameter for determining the mass transfer for carbon dioxide (CO_2) capture via the chemical absorption process in a packed column, and thus the overall capture efficiency of the packed column. Most of the widely used empirical and semi-empirical models for interfacial area were derived indirectly through absorption mass transfer with simplifications based on fast chemical kinetics. A comprehensive unique multiscale approach to develop a surrogate model for effective mass transfer area in structured packed columns has developed accounting local hydrodynamics as well as variation in physical properties, and changes in solid surface characteristics. The effective contact angle on the packing surface, which describes the packing surface and solvent interaction, was measured using the modified Wilhelmy plate method accounting the physical properties of solvent, CO_2 loading, and temperatures. Next, a comprehensive CFD simulation campaign based on the design of experiments (DOE) were performed to derive a surrogate model of the effective mass transfer area that takes into consideration the physical properties of solvent, contact angle, local hydrodynamics, etc.

The developed algebraic surrogate model was integrated into the ASPEN PLUS process modelling via a FORTRAN subroutine in form of .dll file. The surrogate model integrated into process modelling considers the effective mass transfer area in order to capture CO_2 absorption in each stage of the column. The present multiscale approach has advantage of two-way coupling i.e. interchanging information both direction: 1, ASPEN PLUS to surrogate model (temperature, physical properties, CO_2 loading, etc., at each stage) and 2. Surrogate model computes the effective mass transfer area for

determining CO_2 absorption. This unique and promising capability can aid process modeling to accelerating the carbon capture technology at column scale, particularly supporting large scale pilot experiments.

Reference

1. (WMO), W.M.O., *The Global Climate 2011-2020, A decade of accelerating climate change*. 2023, WMO: Geneva, Switzerland. p. 60.
2. UNFCCC. *The Paris Agreement*. in *UN Climate Change Conference (COP21)*. 2015. Paris, France: United Nations.
3. Razi, N., O. Bolland, and H. Svendsen, *Review of design correlations for CO2 absorption into MEA using structured packings.* International Journal of Greenhouse Gas Control, 2012. **9**(0): p. 193-219.
4. Spiegel, L. and W. Meier, *Distillation Columns with Structured Packings in the Next Decade.* Chemical Engineering Research and Design, 2003. **81**(1): p. 39-47.
5. Mackowiak, J., *Fluid Dynamics of Packed Columns*. 2010, Berlin: Springer-Verlag.
6. Raynal, L., F. Ben Rayana, and A. Royon-Lebeaud, *Use of CFD for CO(2) absorbers optimum design : from local scale to large industrial scale.* Greenhouse Gas Control Technologies 9, 2009. **1**(1): p. 917-924.
7. Raynal, L. and A. Royon-Lebeaud, *A multi-scale approach for CFD calculations of gas–liquid flow within large size column equipped with structured packing.* Chemical Engineering Science, 2007. **62**(24): p. 7196-7204.
8. Tsai, R.E., *Mass Transfer Area of Structured Packing*, in *Chemical Engineering*. 2010, The University of Texas at Austin: Austin, TX. p. 400.
9. Tsai, R.E., et al., *Influence of Surface Tension on Effective Packing Area.* Industrial & Engineering Chemistry Research, 2008. **47**(4): p. 1253-1260.
10. Tsai, R.E., et al., *Influence of viscosity and surface tension on the effective mass transfer area of structured packing.* Energy Procedia, 2009. **1**(1): p. 1197-1204.
11. Tsai, R.E., et al., *A dimensionless model for predicting the mass-transfer area of structured packing.* AIChE Journal, 2011. **57**(5): p. 1173-1184.
12. Janzen, A., et al., *Investigation of liquid flow morphology inside a structured packing using X-ray tomography.* Chemical Engineering Science, 2013. **102**: p. 451-460.
13. Shojaee, S., et al., *Prediction of the Effective Area in Structured Packings by Computational Fluid Dynamics.* Industrial & Engineering Chemistry Research, 2011. **50**(18): p. 10833-10842.
14. Subramanian, K. and G. Wozny, *Analysis of Hydrodynamics of Fluid Flow on Corrugated Sheets of Packing.* International Journal of Chemical Engineering, 2012. **2012**: p. 13.
15. Jammula, A.K., *New Liquid Holdup, Load Point and Flooding Velocity Models in Different Regions of Operations for a Structured Packed Column*, in *Chemical Engineering*. 2014, Oklahoma State University: Stillwater, OK p. 164.
16. Haroun, Y., L. Raynal, and P. Alix, *Prediction of effective area and liquid hold-up in structured packings by CFD.* Chemical Engineering Research and Design, 2014. **92**(11): p. 2247-2254.
17. Sebastia-Saez, D., et al., *Meso-scale CFD study of the pressure drop, liquid hold-up, interfacial area and mass transfer in structured packing materials.* International Journal of Greenhouse Gas Control, 2015. **42**: p. 388-399.
18. Singh, R.K., J.E. Galvin, and X. Sun, *Multiphase flow studies for microscale hydrodynamics in the structured packed column.* Chemical Engineering Journal, 2018. **353**: p. 949-963.
19. Ataki, A. and H.J. Bart, *Experimental and CFD simulation study for the wetting of a structured packing element with liquids.* Chemical Engineering & Technology, 2006. **29**(3): p. 336-347.
20. Singh, R.K., et al., *Hydrodynamics of countercurrent flows in a structured packed column: Effects of initial wetting and dynamic contact angle.* Chemical Engineering Journal, 2020. **398**: p. 125548.
21. Fourati, M., V. Roig, and L. Raynal, *Experimental study of liquid spreading in structured packings.* Chemical Engineering Science, 2012. **80**: p. 1-15.

22. Snoeijer, J.H. and B. Andreotti, *A microscopic view on contact angle selection.* Physics of Fluids, 2008. **20**(5): p. 057101.
23. Shi, M.G. and A. Mersmann, *Effective interfacial area in packed columns.* German chemical engineering, 1985. **8**(2): p. 87-96.
24. Singh, R.K., J.E. Galvin, and X. Sun, *Three-dimensional simulation of rivulet and film flows over an inclined plate: Effects of solvent properties and contact angle.* Chemical Engineering Science, 2016. **142**: p. 244-257.
25. Kohrt, M., et al., *Texture influence on liquid-side mass transfer.* Chemical Engineering Research and Design, 2011. **89**(8): p. 1405-1413.
26. Wenzel, R.N., *Resistance of solid surfaces to wetting by water.* Industrial & Engineering Chemistry, 1936. **28**(8): p. 988-994.
27. Nicolaiewsky, E.M.A. and J.R. Fair, *Liquid Flow over Textured Surfaces. 1. Contact Angles.* Industrial & Engineering Chemistry Research, 1998. **38**(1): p. 284-291.
28. Singh, R.K., J.E. Galvin, and X. Sun, *Hydrodynamics of the rivulet flow over corrugated sheet used in structured packings.* International Journal of Greenhouse Gas Control, 2017. **64**: p. 87-98.
29. Chau, T.T., et al., *A review of factors that affect contact angle and implications for flotation practice.* Adv Colloid Interface Sci, 2009. **150**(2): p. 106-15.
30. Singh, R.K., et al., *Experimental measurement of the effective contact angle for solvent/packing interactions in a structured packed column for CO2 capture*. 2023, Pacific Northwest National Laboratory: United States. p. 1 - 33.
31. Fu, Y., et al., *Determination of effective contact angle for CO2 capture column packing coupons with Wilhelmy plate experiments.* . 2021, Pacific Northwest National Laboratory: United States. p. 1 - 33.
32. Iso, Y., et al., *Numerical and Experimental Study on Liquid Film Flows on Packing Elements in Absorbers for Post-combustion CO2 Capture.* Energy Procedia, 2013. **37**(0): p. 860-868.
33. Siemens, D.I.S., *Simcenter STAR-CCM+, version 2210* 2022, Siemens Product Lifecycle Management Software Inc: USA.
34. Hirt, C.W. and B.D. Nichols, *Volume of fluid (VOF) method for the dynamics of free boundaries.* Journal of Computational Physics, 1981. **39**(1): p. 201-225.
35. Hinze, J.O., *Turbulence*. 2 ed. 1975: McGraw-Hill. 790.
36. Brackbill, J.U., D.B. Kothe, and C. Zemach, *A continuum method for modeling surface tension.* Journal of Computational Physics, 1992. **100**(2): p. 335-354.
37. Joly, J.F., et al., *CFD Applied to Process Development in the Oil and Gas Industry – A Review.* Oil & Gas Science and Technology – Revue d'IFP Energies nouvelles, 2015. **71**(3): p. 42.
38. Dybbs, A. and R.V. Edwards, *A New Look at Porous Media Fluid Mechanics — Darcy to Turbulent*, in *Fundamentals of Transport Phenomena in Porous Media*, J. Bear and M.Y. Corapcioglu, Editors. 1984, Springer Netherlands: Dordrecht. p. 199-256.
39. Menter, F.R., *Two-equation eddy-viscosity turbulence models for engineering applications.* AIAA Journal, 1994. **32**(8): p. 1598-1605.
40. Höhne, T. and J.-P. Mehlhoop, *Validation of closure models for interfacial drag and turbulence in numerical simulations of horizontal stratified gas–liquid flows.* International Journal of Multiphase Flow, 2014. **62**(0): p. 1-16.
41. Owens, S.A., et al., *Computational Fluid Dynamics Simulation of Structured Packing.* Industrial & Engineering Chemistry Research, 2013. **52**(5): p. 2032-2045.
42. Singh, R.K., C. Wang, and Z. Xu, *Residence time distribution in a structured packing unit for monitoring aerosol emissions.* International Journal of Greenhouse Gas Control, 2018. **79**: p. 181-192.
43. Raynal, L., C. Boyer, and J.-P. Ballaguet, *Liquid Holdup and Pressure Drop Determination in Structured Packing with CFD Simulations.* The Canadian Journal of Chemical Engineering, 2004. **82**(5): p. 871-879.

44. Khosravi Nikou, M.R. and M.R. Ehsani, *Turbulence models application on CFD simulation of hydrodynamics, heat and mass transfer in a structured packing.* International Communications in Heat and Mass Transfer, 2008. **35**(9): p. 1211-1219.
45. Friedman, J.H., *Multivariate Adaptive Regression Splines.* The Annals of Statistics, 1991. **19**(1): p. 1-67, 67.
46. Fu, Y., et al., *The influence of random packed column parameters on the liquid holdup and interfacial area.* AIChE Journal, 2022: p. e17691.
47. Green, C.W., et al., *Novel Application of X-ray Computed Tomography: Determination of Gas/Liquid Contact Area and Liquid Holdup in Structured Packing.* Industrial & Engineering Chemistry Research, 2007. **46**(17): p. 5734-5753.
48. Singh, R.K., et al., *Hydrodynamics of countercurrent flow in an additive manufactured column with triply periodic minimal surfaces for carbon dioxide capture.* Chemical Engineering Journal, 2022. **450**: p. 138124.
49. Singh, R.K., et al. *Numerical Simulation for Interfacial Forces of Counter-Current Flow over an Inclined Plate*. in *12th International Conference on Gas-Liquid & Gas-Liquid-Solid Reactor Engineering (GLS12)*. 2015. AIChE.
50. Singh, R.K., et al., *Breakup of a liquid rivulet falling over an inclined plate: Identification of a critical Weber number.* Physics of Fluids, 2017. **29**(5): p. 052101.
51. Fu, Y., et al., *Investigation of countercurrent flow profile and liquid holdup in random packed column with local CFD data.* Chemical Engineering Science, 2020. **221**: p. 115693.
52. Hoffmann, A., et al., *Fluid dynamics in multiphase distillation processes in packed towers.* Computers & Chemical Engineering, 2005. **29**(6): p. 1433-1437.
53. Nusselt, W., *Die Oberflächenkondesation des Wasserdampfes.* Zeitschrift des Vereines Deutscher Ingenieure 1916. **60**(27): p. 541–546.
54. Wang, C., et al., *Hierarchical calibration and validation framework of bench-scale computational fluid dynamics simulations for solvent-based carbon capture. Part 2: Chemical absorption across a wetted wall column.* Greenhouse Gases: Science and Technology, 2018. **8**(1): p. 150-160.
55. Wang, C., et al., *Hierarchical calibration and validation for modeling bench-scale solvent-based carbon capture. Part 1: Non-reactive physical mass transfer across the wetted wall column.* Greenhouse Gases: Science and Technology, 2017. **7**(4): p. 706-720.
56. Wang, C., et al., *Beyond the standard two-film theory: Computational fluid dynamics simulations for carbon dioxide capture in a wetted wall column.* Chemical Engineering Science, 2018. **184**: p. 103-110.
57. Haroun, Y., L. Raynal, and D. Legendre, *Mass transfer and liquid hold-up determination in structured packing by CFD.* Chemical Engineering Science, 2012. **75**: p. 342-348.
58. Eslick, J.C., et al., *A Framework for Optimization and Quantification of Uncertainty and Sensitivity for Developing Carbon Capture Systems.* Energy Procedia, 2014. **63**: p. 1055-1063.